mater.scichina.com link.springer.com Published online 12 April 2024 | https://doi.org/10.1007/s40843-023-2774-8

Inhibiting PI3K/AKT/mTOR signaling by metal-organic frameworks for overcoming multiple drug resistance in chemoradiotherapy

Chunyu Song[1†], Xue Guan[2†], Changming Xie[3†], Shan Jiang[4], Zhiwen Hong[4], Qiong Wu[5], Guofan Qu[1*], Tengchuang Ma[4*] and Yali Cui[4*]

ABSTRACT **Angiogenesis in the tumor microenvironment is the main cause for the insensitivity of tumor cells to chemoradiotherapy. Strategies for increasing the sensitivity of tumor cells to conventional therapies using nanoparticles are limited. In this study, we developed rationally designed microenvironment response nanoparticles with physicochemical and biological features to overcome cisplatin resistance by using decomposition product from Zr-metal–organic framework (MOF) to inhibit the phosphatidylinositol 3-kinase (PI3K)/AKT/mammalian target of rapamycin (mTOR)/vascular endothelial growth factor (VEGF) pathway in chemoradiotherapy. Cisplatin (CDDP) is encapsulated into Zr-MOF and bovine serum albumin (BSA) is modified into the surface of nanoparticles to create CDDP@Zr-MOF-BSA (abbreviated as CDDP@Zr-MOF), which acts as an excellent radiosensitizer and exhibits microenvironment response, preferable tumor accumulation, high-efficiency inhibition of angiogenesis, and obviously reduced efflux on resistant A549 cells. The rate of angiogenesis inhibition in the combined treatment group is 6-fold higher than that in other control groups. Moreover, CDDP@Zr-MOF not only increases the therapeutic effect remarkably, but also regulates the tumor microenvironment and inhibits the expression of a drug-efflux transporter, namely multidrug resistance-associated protein 1 (MRP1), for reversing drug resistance in A549R cells. Thus, CDDP@Zr-MOF causes synergistic cytotoxicity in A549R cells, and high-efficiency eradication of cisplatin-resistant tumor without regrowth by inhibiting angiogenesis in the tumor microenvironment. The microenvironment responsiveness of CDDP@Zr-MOF provides a multipurpose synergistic approach for treating drug-resistant tumors with chemoradiotherapy.**

Keywords: angiogenesis, multidrug resistance, radiotherapy, Zr-MOF, microenvironment

INTRODUCTION

Chemotherapeutic drug resistance remains a major obstacle in curing cancer [1–3]. Cisplatin and its derivatives, the most commonly used chemicals for treating lung cancer are not clinically satisfactory due to drug resistance [4–8]. Cisplatin resistance is a multi-factorial phenomenon that renders treatment inefficient [9–12]. For example, insufficient intracellular drug accumulation, owing to low cellular uptake and high cellular efflux, is the main concern for cisplatin resistance [13–15]. Poor absorption, increase in biotransformation, or excretion of chemotherapeutics leads to low blood concentration of the drug, thereby reducing drug diffusion to cancer cells [16–18]. Furthermore, intracellular thiol-containing species, such as glutathione (GSH) and metallothionein (MT), may strongly bind and sequester cisplatin. Studies have reported that the chemosensitivity of lung cancer cells to cisplatin can be restored by reducing the cellular concentration of GSH. Xu *et al.* [19] demonstrated that sulforaphane mediates GSH depletion through polymeric nanoparticles to restore cisplatin chemosensitivity and enhance treatment efficacy. In addition, chemical-mediated apoptosis and DNA damage can be repaired. Due to the presence of DNA damage repair pathways, homologous recombination repair occurs after DNA damage, maintaining the ability of tumor cells to proliferate, invade, and metastasize, leading to insensitivity to chemotherapy drugs [20–22]. Although multiple factors influence chemotherapeutic drug resistance, mechanisms involved in determining drug resistance remain unclear.

Recently, the intrinsic and acquired dysfunction of specific pathways was identified as the cause of drug resistance. Activated angiogenic pathways, such as phosphatidylinositol 3-kinase (PI3K)/AKT/mammalian target of rapamycin (mTOR)/vascular endothelial growth factor (VEGF) and hypoxia-inducible factor-l alpha (HIF1α)/carbonic anhydrase IX (CAIX)/VEGF are known to be associated with drug resistance [23,24]. Activation of the PI3K/AKT/mTOR/VEGF pathway can induce

[1] Department of Orthopedics, Harbin Medical University Cancer Hospital, Harbin 150081, China
[2] Animal Laboratory Center, The Second Affiliated Hospital of Harbin Medical University, Harbin 150081, China
[3] Department of Thyroid Surgery, Key Laboratory of Hepatosplenic Surgery, Ministry of Education, The First Affiliated Hospital of Harbin Medical University, Harbin 150007, China
[4] Department of Nuclear Medicine, Harbin Medical University Cancer Hospital, Harbin 150081, China
[5] Laboratory of Controllable Preparation and Application of Nanomaterials, Key Laboratory of Cryogenics, Technical Institute of Physics and Chemistry, Chinese Academy of Sciences, Beijing 100190, China
† These authors contributed equally to this work.
* Corresponding authors (emails: guofanqu@126.com (Qu G); matengchuang1988@126.com (Ma T); yalicui68@126.com (Cui Y))

disordered hyperangiogenesis, increase tumor cell proliferation, and decrease apoptotic activity, thereby promoting tumor growth and progression. Increased incidence of drug resistance due to PI3K/AKT/mTOR/VEGF pathway activation is the most important reason for treatment failure [25–27]. Several reasons for the association between the hyperangiogenic pathway and drug resistance in tumor cells exist. Activation of the PI3K/AKT/mTOR/VEGF pathway can lead to the overexpression of drug-resistant proteins, namely multidrug resistance-associated protein 1 (MRP1) as the most representative, which increases chemotherapeutic drug efflux into cells, thereby leading to drug resistance [28]. First, tumor vasculature is non-homogeneous, tortuous, and highly permeable. This leads to tumor tissue heterogeneity, and aggravates hypoxia status, which cause the upregulation of the HIF-1α/CAIX/VEGF pathway, ultimately affecting chemotherapeutic treatment [29–31]. Overactivation of the PI3K/AKT/mTOR/VEGF pathway contributes to a heterogeneous vascular system, causing insensitivity of tumor cells to chemotherapeutics and drug resistance [32–34]. In addition, the balance between proteases and their inhibitors is important for maintaining tumor homeostasis. The disruption between them induced by tumor-related vascular endothelial cells, which can remodel the microenvironment for tumor growth, activates PI3K/AKT/mTOR/VEGF and HIF-1α/CAIX/VEGF pathways, thereby exacerbating drug resistance. Finally, VEGF secretion in tumor cells can induce angiogenesis, affect the efficacy of anti-angiogenic inhibitors in patients to promote VEGF binding in tumor cells by a feed-forward manner, initiate PI3K/AKT/mTOR/VEGF and HIF-1α/CAIX/VEGF signaling, and result in the progress of drug resistance [35–37]. Therefore, PI3K/AKT/mTOR/VEGF and HIF-1α/CAIX/VEGF signaling pathways are targets in antiangiogenesis studies, and reversion of drug resistance can be achieved by inhibiting these pathways [38–40].

Multiple upstream and downstream regulatory molecules are present in PI3K/AKT/mTOR and HIF-1α/CAIX/VEGF pathways. Inhibiting these pathways can decrease tumor cell proliferation, induce tumor cell apoptosis, and reverse drug resistance [41,42]. Multidrug resistance has been reversed by using similar derivatives or isozymes of each target as inhibitors, such as the PI3K inhibitor [43], HIF-1α inhibitor [44], and VEGF inhibitor [45]. However, due to the relatively low inhibition efficiency, target inhibitor strategies have not achieved desired results for interfering with PI3K/AKT/mTOR and HIF-1α/CAIX/VEGF signalling. Studies focusing on nano-drug delivery systems as carriers, loaded with target inhibitors and chemotherapy drugs for combating drug resistance by targeting angiogenic pathways, have been reported. Nie's group [46–48] reported that the use of metal–organic framework (MOF) nanoparticles containing the VEGF inhibitor combined with photodynamic therapy, significantly reduced vessel density and VEGF levels, inhibited angiogenic pathway activation, and increased tumor cell sensitivity to chemotherapeutics. Because angiogenic pathways are associated with drug resistance, reversing crucial pathways involved in drug resistance, such as PI3K/AKT/mTOR/VEGF and HIF-1α/CAIX/VEGF, using nano-drug delivery systems has great potential.

Despite these advancements, cisplatin drugs succumb to the emergence of acquired resistance due to failure in inhibiting factors involved in the PI3K/AKT/mTOR/VEGF pathway. Because of the presence of correlation target in the two pathways, the HIF1α/CAIX/VEGF pathway has gained increasing attention. In 2019, we demonstrated a hypoxia microenvironment regulating nano-drug delivery system [49]. Inspired by the CAIX inhibition function of Zr-MOF degradation products, we encapsulated cisplatin (CDDP) into Zr-MOF and modified it using bovine serum albumin (BSA) to obtain CDDP@Zr-MOF-BSA (abbreviated as CDDP@Zr-MOF) for destroying cisplatin-resistant tumor (A549R). In this study, CDDP@Zr-MOF exhibited multistage and cascade-responsive advantages as an efficient vehicle: (1) degradation products from Zr-MOF inhibited the expression of CAIX effectively and improved the hypoxic environment. (2) CAIX triggered the downregulation of HIF1α/CAIX/VEGF and blocked PI3K/AKT/mTOR/VEGF signalling. (3) MRP1, which is associated with the PI3K/AKT/mTOR/VEGF pathway, can be controlled further and realize the reversion of cisplatin in A549R cells (Scheme 1). Moreover, we introduced radiotherapy (RT) for collaborative treatment on account of the previously used microenvironment modulation strategy. Consequently, CDDP@Zr-MOF + RT generated synergistic cytotoxicity against A549R cells by a cascade

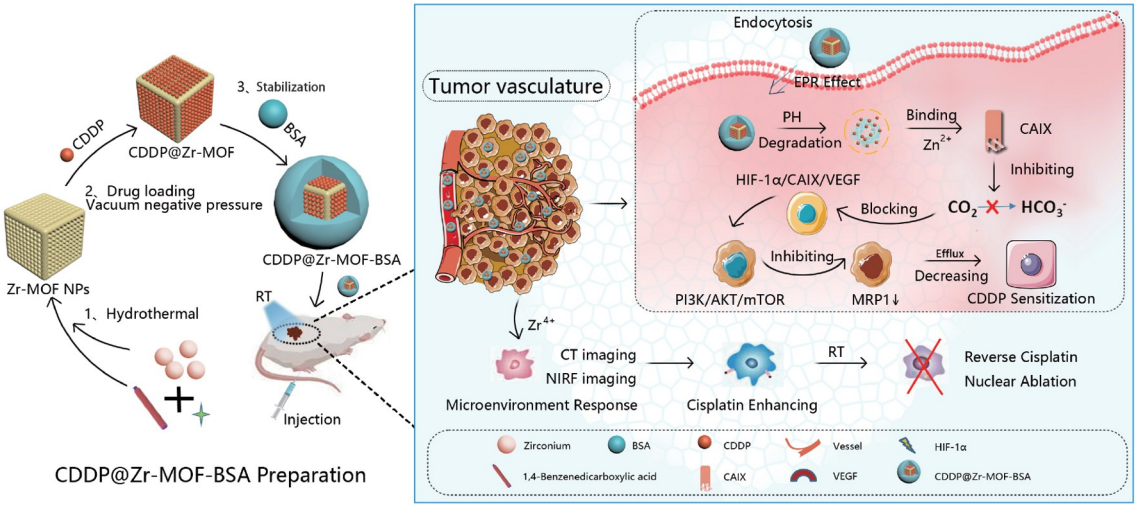

Scheme 1 Schematic of the composition of CDDP@Zr-MOF nanocomposites and the therapeutic principle based on CDDP@Zr-MOF + RT mediated angiogenesis inhibition mechanism for reversing drug resistance in tumor microenvironment.

microenvironment-responsive nano-drug-delivery platform, thus providing a new promising treatment strategy for cisplatin-resistant tumors.

EXPERIMENTAL SECTION

Synthesis of the CDDP@Zr-MOF

Zr-MOF was synthesized *via* one step with a hydrothermal method. 33.8 mg of zirconium tetrachloride, 24.0 mg of 1,4-benzenedicarboxylic acid, and 18.9 mg of polyvinyl pyrrolidone were weighed and added into 33.4 mL of *N*,*N*-dimethylformamide for ultrasonic dispersion dissolution. Then, it was put into the polyethylene hydrothermal reactor and reacted at 120°C for 10 h. At the end of the reaction, the reaction liquid was centrifuged, sub-layer precipitation was washed with ethanol three times, and the final product Zr-MOF was collected. CDDP was loaded into Zr-MOF by the vacuum negative pressure method to synthesize CDDP@Zr-MOF. Specifically, Zr-MOF (10 mg) was dispersed into 5 mL DMF, which was evenly dispersed by ultrasound. The same amount of CDDP was added, which was also uniformly dissolved by ultrasound. The mixture was kept under vacuum until the solution was drained. The precipitant was washed alternately with dH_2O and ethanol three times to obtain CDDP@Zr-MOF. To improve biocompatibility, BSA was coated on the surface of CDDP@Zr-MOF; 5 mg BSA was added to the aqueous solution containing 10 mg of CDDP@Zr-MOF with stirring for 30 min. CDDP@Zr-MOF-BSA was obtained by centrifuging and washing with water three times.

Characterization

Transmission electron microscopy (TEM) was performed using the A JEOL JEM 2100F electron microscope at 200 kV. Zeta-Sizer (Malvern Nano series) was used to acquire the hydrodynamic diameter, and Excalibur 3100 (Varian) was performed to test Fourier transform infrared (FTIR) spectra.

Radiotherapy experiments

A549R cells and cisplatin-resistant mice models were treated with image guided RT, which was a linear accelerator equipment with an X-ray dose of 8 Gy for 2 min.

Transwell assay and hoechst 33258 staining

After treatment for 48 h, A549R cells were seeded on top of a Matrigel-coated invasion chamber (1×10^6) in serum-free RPMI-1640, and fetal bovine serum (FBS) containing RPMI-1640 was added to the lower chamber. After 24 h, cells on the bottom of the upper compartment were fixed by using 4% paraformaldehyde for 30 min. After staining with 0.1% crystal violet for 15 min, the chambers were photographed under a microscope (Olympus, Tokyo, Japan). The Hoechst 33258 staining was performed as previously method.

γ-H_2AX immunofluorescence and colony formation assay

This section of the experiment was carried out with reference to the standard procedure as reported [21]. Three independent experiments were performed.

NIRF imaging *in-vivo*

Near-infrared fluorescence (NIRF) imaging of A549R tumor-bearing mice was performed by using an *in-vivo* Imaging System (Bruker, German). CDDP@Zr-MOF-cy5.5 (10 mg kg^{-1}, in 5% *D*-glucose dissolved in ddH_2O) was injected *via* the tail vein and NIRF imaging was catched (excitation = 710 nm; emission = 750 nm) at 0, 1, 6, 12, and 24 h. Average NIRF intensities were managed to express photon signals in tumors at different times according to the tumor.

CT imaging *in-vivo*

We used animal micro-computed tomography (CT) scanner for CT imaging (Quantum GX, PerkinElmer). A549R tumor-bearing mice were examined by micro-CT imaging at 0, 1, 6, 12, and 24 h. The dosage of CDDP@Zr-MOF administered was 10 mg kg^{-1} (body weight) *via* tail vein. The scanning parameters as followed: voltage: 90 kV; current: 80 μA; acquisition field of view (FOV): 72 mm × 40 mm. The three-dimensional (3D) reconstruction was established and analyzed by using an Analyze 12.0 software.

Antiangiogenesis mediated by CDDP@Zr-MOF + RT *in-vivo*

All the mice treatments were approved by Harbin Medical University Cancer Hospital. For xenograft implantation, a total of 5×10^6 A549R cells were injected subcutaneously into the back next to the left forelimb of 4-week-old female BALB/c mice (Charles River Laboratories, Beijing, China), for all of which tumors with a size of 30–50 mm^3 were developed within 7–10 d. All the A549R mice were then randomly assigned to seven groups (6 mice/group) and classified by intravenous administration of nanomaterials, and then irradiated or not irradiated with X-ray. Mice weight and tumor volume were measured every day. Tumor volume was calculated as (length × $width^2$)/2. After 3 weeks, we removed the tumor and main organs to calculate the therapeutic effect of the seven groups.

TUNEL and immunohistochemical staining

We used standard techniques to test pathologic changes for all tumors and other organs in the seven groups. All tumor tissues were used for H&E staining, and terminal deoxynucleotidyl transferase-mediated dUTP nick end-labeling (TUNEL) staining and immunohistochemistry staining were performed. All sections were observed by using a microscope.

Western blotting analysis

Relative protein concentration was quantified using the BCA protein assay kit as our described previously [40]. The primary antibodies were CAIX, PI3K, Akt, mTOR, VEGF, MRP1, and β-actin, and the secondary antibody was anti-rabbit IgG. Protein bands were imaged using the chemiluminescence system (Tanon-5200, China) and quantitative data were managed by Image J.50 software.

Ethical approval

All animal experiments were carried out in accordance with the agreement of Harbin Medical University Cancer Hospital (No: SYXK2019-001; SCXK2019-001). All the animal experimental operations were in compliance with the National Guidelines for Animal Protection.

RESULTS AND DISCUSSION

Synthesis and characterization of CDDP@Zr-MOF

Zr-MOF was synthesized by a one-step hydrothermal process. The synthesized Zr-MOF has a uniform particle size and good

monodispersity, which can be seen in TEM images (Fig. 1a). We introduced BSA into the surface of CDDP@Zr-MOF to fabricate the CDDP@Zr-MOF-BSA. Analyses of the scanning electron microscopy image are shown in Fig. S1a, b. The average size of Zr-MOF is 80 ± 10 nm (Fig. S1e), which further confirms monodispersity. The average hydrodynamic particle size of Zr-MOF is 155 nm, which was measured using dynamic light scattering (Fig. 1b). CDDP was loaded into Zr-MOF through the vacuum negative pressure method to synthesize CDDP@Zr-MOF. Energy-dispersive X-ray spectroscopy of CDDP@Zr-MOF reveals the content of each element (Fig. S1f), whereas high-resolution TEM (HRTEM) mapping of CDDP@Zr-MOF reveals the elemental distribution of Zr, Pt, O, C, and N (Fig. 1c), indicating that CDDP was successfully loaded into Zr-MOF. We used FTIR spectroscopy to evaluate CDDP loading into Zr-MOF (Fig. 1d). The characteristic amine stretching vibration peak of CDDP between 3400 and 3200 cm^{-1} appeared in the CDDP@Zr-MOF spectrum. Powder X-ray diffraction (PXRD) patterns of both Zr-MOF and CDDP@Zr-MOF indicate excellent crystallinity (Fig. 1e). The peaks of Zr-MOF and CDDP@Zr-MOF overlapped well, and differences were also observed, manifesting successful CDDP loading. Zeta potential values for Zr-MOF, CDDP@Zr-MOF, and CDDP@Zr-MOF-BSA were −17.6, −20.1, and 4.5 mV, respectively (Fig. S1d), further validating the

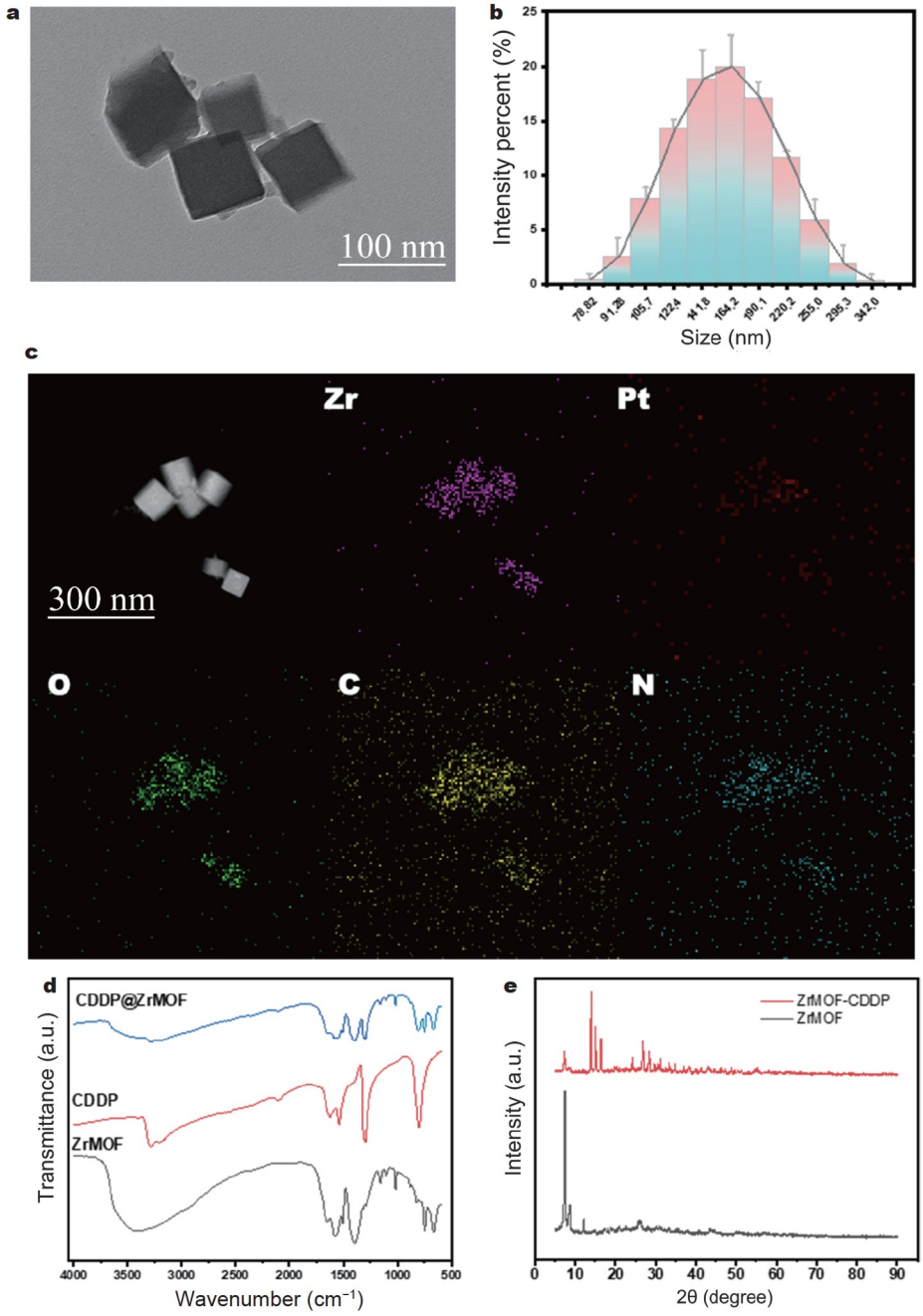

Figure 1 (a) TEM image of Zr-MOF. (b) Average hydrodynamic particle size of Zr-MOF. (c) HRTEM image of CDDP@Zr-MOF in dark field and the relative element mapping for zirconium, platinum, oxygen, carbon, and nitrogen. Scale bar is 300 nm. (d) FTIR spectrometry of Zr-MOF, CDDP, and CDDP@Zr-MOF. (e) PXRD patterns of Zr-MOF and CDDP@Zr-MOF.

CDDP@Zr-MOF-BSA composition.

Evaluation of biological behavior changes induced in A549R cells by CDDP@Zr-MOF + RT

Before demonstrating the mechanism of CDDP@Zr-MOF + RT in reversing cisplatin resistance in A549R cells, we evaluated the effect of CDDP@Zr-MOF + RT on changes in the biological behavior of A549R cells. To improve the biocompatibility of the nano-drug system, BSA was modified on CDDP@Zr-MOF surface to obtain CDDP@Zr-MOF-BSA before performing experiments (abbreviated as CDDP@Zr-MOF). The A549R cells were divided into seven groups, including control, cisplatin, RT, Zr-MOF, CDDP@Zr-MOF, Zr-MOF + RT, and CDDP@Zr-MOF + RT. Cell proliferation ability, apoptosis rate, and invasion ability were assessed and compared among these groups. We evaluated the ability of CDDP@Zr-MOF + RT to affect the biological activity of A549R cells by performing the methyl thiazolyl tetrazolium (MTT) assay. For these assays, A549R and A549 cell lines were used. Nanomaterials and drugs were co-cultured with A549R and A549 cells for 24 and 48 h, respectively. The combined group exhibited less cellular stability than other treatments at two time points (Fig. S2, and Fig. 2a, b). Thus, CDDP@Zr-MOF + RT can inhibit proliferation of A549R and A549 cells, whereas the ability to inhibit tumor proliferation by the other six groups was unsatisfactory. We evaluated therapeutic outcomes of CDDP@Zr-MOF + RT using the clonogenic assay and found 89.4%, 82.1%, 65.6%, 84.1%, and 62.1% colony formation in control, cisplatin, RT, Zr-MOF, and CDDP@Zr-MOF groups of A549R cells, respectively. However, only 45.2% and 19.8% A549R cells survived in the Zr-MOF + RT and CDDP@Zr-MOF + RT groups, respectively (Fig. 2c, e). Results from the clonogenic assay in A549 cells revealed similar results (Fig. S3). Thus, CDDP@Zr-MOF can overcome cisplatin resistance for increasing the sensitivity of A549R to chemotherapy. Results from the transwell assay to detect the invasion ability of A549R cells revealed that CDDP@Zr-MOF + RT could inhibit invasion of A549R cells. Increased entry of chemotherapeutic drugs into A549R and A549 cells to kill them, thereby reduces their ability to invade (Fig. S4, and Fig. 2d, f). Hoechst staining revealed marked apoptosis in combination group than other groups, and a distinctly broken fragment of the nucleus was observed in combination therapy (Fig. S5, and Fig. 2g, j). Finally, immunofluorescence was used to evaluate γ-H_2AX foci in A549R nuclei for quantifying DNA double-strand breaks. Conspicuous green fluorescence was observed in the CDDP@Zr-MOF + RT group. A spot of γ-H_2AX fluorescence signal was observed in control, cisplatin, RT, and Zr-MOF groups. Compared with these four groups, CDDP@Zr-MOF and Zr-MOF + RT displayed relatively high numbers of γ-H_2AX foci. High γ-H_2AX intensity in the combination group indicated more DNA damage. Number of γ-H_2AX foci/100 μm^2 for the combination group was 2.96-, 2.08-, and 1.44-fold higher than that in RT, Zr-MOF@CDDP, and Zr-MOF + RT groups, respectively. The combination group demonstrated the difference compared with the control group ($p < 0.001$), compared with cisplatin, RT, and Zr-MOF groups ($p < 0.01$), and compared with CDDP@Zr-MOF, Zr-MOF + RT groups ($p < 0.05$) (Fig. S6, Fig. 2h, i). CDDP@Zr-MOF mediated RT can effectively inhibit the proliferation and invasion ability of A549R cells, and then promote apoptosis in tumor cells. These changes in biological behavior were attributed to the increased infiltration of cisplatin into the target site and susceptibility of A549R cells. Random angiogenesis in the microenvironment is an important barrier for tumor cells to resist cisplatin. The activation of angiogenic pathways further increases cisplatin tolerance in cells. Furthermore, 1,4-benzenedicarboxylic acid, derived from Zr-MOF biodegradation, can bind to Zn^{2+} functional in CAIX tightly in an acidic tumor microenvironment to downregulate hypoxia, as reported by our group [44]. HIF1α/CAIX/VEGF signaling is blocked and VEGF stimulated growth is inhibited. Zr-MOF mediated VEGF inhibition can inhibit PI3K/AKT/mTOR/VEGF signaling through a cascade reaction, which is associated with the expression of the MRP1 as a drug-efflux transporter. As a microenvironment response nanomaterial, CDDP@Zr-MOF + RT can further inhibit PI3K/AKT/mTOR/VEGF angiogenic pathway in positive feedback manner regulation synergistically, thereby inactivating MRP1, increasing the rate of cisplatin retention and sensitivity in A549R cells, reversing drug resistance, and increasing A549R cell apoptosis and death combined with RT. The ability of A549R cells to proliferate, invade, and apoptosis can be regulated by CDDP@Zr-MOF + RT. The combination treatment provided a strategy to modulate tumor microenvironment, reduce drug resistance, and generate synergistic cytotoxicity, and thus, inhibited A549R cell regrowth. We speculated that CDDP@Zr-MOF + RT could act as VEGF inhibitor, thereby inhibiting HIF-1α/CAIX/VEGF and PI3K/Akt/mTOR/VEGF signaling in tumor cells, and thus, improving the sensitivity of tumor cells to cisplatin by decreasing MRP1 expression. Furthermore, we used apatinib which is vascular endothelial growth factor receptor 2 (VEGFR2) inhibitor. Apatinib can highly selectively inhibit the binding site of VEGFE-2 and ATP, block downstream signal transduction, inhibit tumor angiogenesis, and then reduce the ability of tumor cell proliferation, invasion and metastasis. We used apatinib as a positive control to verify its ability to inhibit the PI3K/AKT/mTOR/VEGF pathway. A549R cells were divided into four groups, namely control, cisplatin, apatinib, and apatinib + CDDP@Zr-MOF + RT. We evaluated the proliferation, invasion, and ability to apoptosis among four groups. Results from the combined treatment group were consistent with other results. Combined treatment effectively changed the biological behavior of A549R cells and had a better curative effect on tumor cells (Figs S7 and S8).

Mechanisms of angiogenesis inhibition mediated by CDDP@Zr-MOF + RT *in-vitro*

CAIX expression was verified in all groups before performing immunofluorescence to quantify two angiogenesis markers. The results showed that significant CAIX inhibition could be observed in the CDDP@Zr-MOF + RT group compared with other treatment groups, indicating that the combined treatment group could effectively regulate the expression of CAIX in the hypoxia microenvironment, thereby improving the hypoxia status and inhibiting hypoxia signaling pathways, such as HIF-1α/CAIX/VEGF (Figs S9 and S10). Platelet endothelial cell adhesion molecule-1 (CD31) and VEGF are blood vessel markers that are used to evaluate angiogenesis in tumor cells. CD31 is primarily used to demonstrate the presence of endothelial tissue and assess tumor angiogenesis, which indicates the extent of a rapidly growing tumor. In various tumors, VEGF overexpression correlates with invasion and metastasis, and positively correlates with tumor malignancy. We used

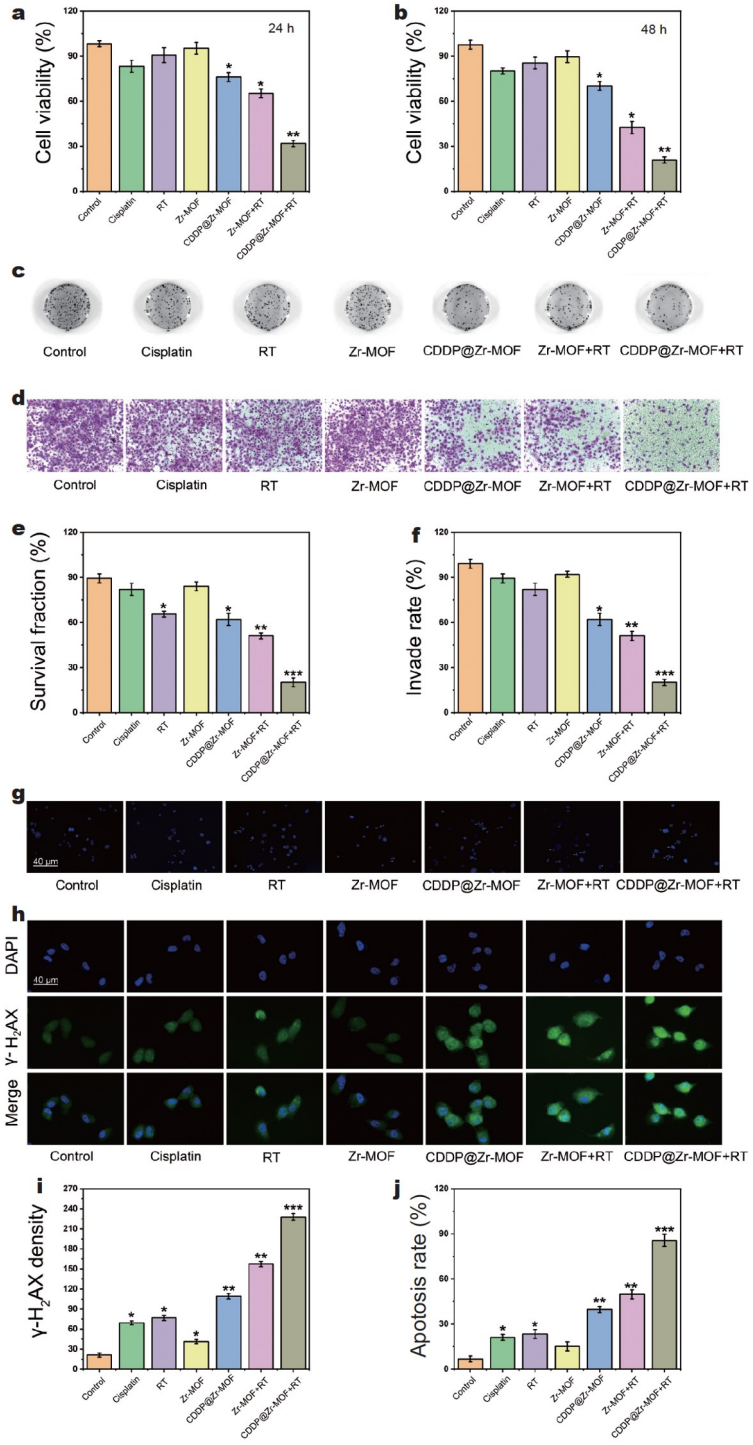

Figure 2 CDDP@Zr-MOF mediated enhancement of chemoradiotherapy effects on the biological behaviors in cisplatin resistant A549 cells. (a, b) MTT assay results of A549R cells in different groups including the control, cisplatin, RT, Zr-MOF, CDDP@Zr-MOF, Zr-MOF + RT, and CDDP@Zr-MOF + RT groups. (c) Colony results of A549R cells treated with cisplatin, Zr-MOF, CDDP@Zr-MOF (100 ppm, 1 mL) combined with RT (X-ray radiation was 8 Gy). (d) Invasion ability and rate of different treatment methods (compared with control group). (e, f) Corresponding survival fraction and relative invade rate evaluation of A549R cells (n = 3). (g) Hoechst images of different groups. (h) Representative immunofluorescence images of nuclear condensation and DNA fragmentation caused by different treatments (100 ppm; 1 mL), and radiation dose was 8 Gy in all groups contained RT. Nuclear visualization was stained with 4′,6-diamidino-2-phenylindole (DAPI) and DNA fragmentation was stained with γ-H_2AX, respectively (green fluorescence intensity represents the degree of nuclear breakdown). (i, j) Counted number of γ-H_2AX and relative apotosis rate of A549R cells in different groups (* represents the statistical difference between the treatment groups and the control group). Data are presented as the mean ± SD. $^{*}p < 0.05$; $^{**}p < 0.01$; $^{***}p < 0.001$.

immunofluorescence to verify the expression of CD31 and VEGF in all groups. The results indicated that the CDDP@Zr-MOF + RT treatment group expressed the least amount of CD31 and VEGF. Compared with control, cisplatin, and RT groups, the inhibition rate of CD31 in the combination treatment group was almost 6-fold in A549R cells (Fig. 3a, c). Furthermore, the

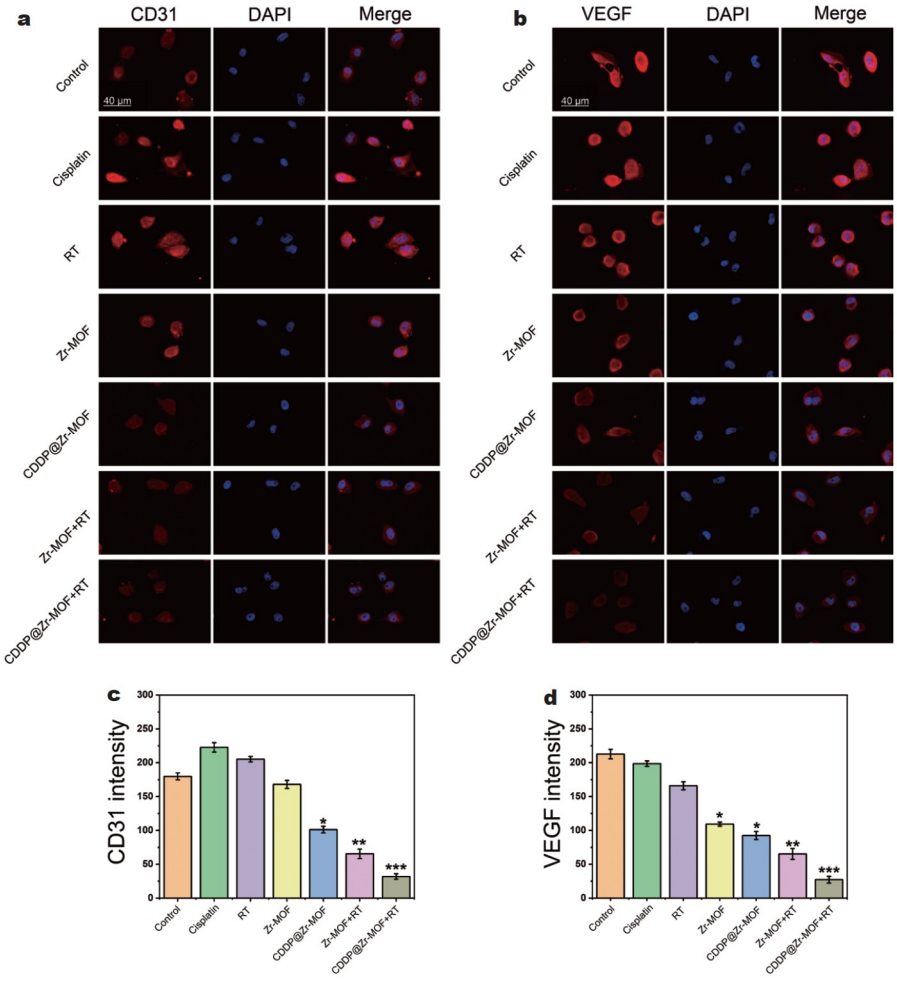

Figure 3 Immunofluorescence suppression results for two angiogenesis markers mediated by CDDP@Zr-MOF + RT in cisplatin resistant A549 cells. (a, b) Representative immunofluorescence images of CD31 and VEGF induced by different treatments (100 ppm; 1 mL), and X-ray radiation was 8 Gy in all groups combined with RT. Nuclear visualization and two angiogenesis markers were stained with DAPI, and CD31 and VEGF, respectively (red fluorescence intensity represents the expression of both two markers). (c, d) Corresponding normalized number of CD31 and VEGF of A549R cells in different groups (* represents the statistical difference between the treatment groups and the control group). Data are presented as the mean ± SD. * $p < 0.05$; ** $p < 0.01$; *** $p < 0.001$.

inhibition rate of VEGF in CDDP@Zr-MOF + RT was nearly 9-, 7-, and 6-fold than control, cisplatin, and RT groups in A549R cells, respectively (Fig. 3b, d). As the main inhibitor of angiogenesis, Zr-MOF can effectively inhibit VEGF, which is the key target of angiogenesis in the tumor microenvironment, promoting the downregulation of tumor cell invasion and metastasis, thereby resulting in tumor cell death. Chemoradiotherapy further increased the ability of Zr-MOF to inhibit VEGF which the PI3K/AKT/mTOR/VEGF pathway was blocked because VEGF is downstream, thereby shutting down the expression of MRP1, which is involved in this pathway. CDDP@Zr-MOF + RT might cause long-term retention of cisplatin in A549R cells and effectively decrease the incidence of cisplatin-resistance through the inhibition of the PI3K/AKT/mTOR/VEGF pathway. Finally, we used apatinib as VEGFR-2 inhibitor to evaluate its anti-angiogenic ability in combination with CDDP@Zr-MOF + RT. Immunofluorescence results revealed that in the apatinib +CDDP@Zr-MOF + RT group, the expression of CD31 and VEGF was induced at a very low level compared with that in other groups in A549R cells, indicating that combination therapy can suppress angiogenesis with high efficiency (Fig. S11).

Based on immunofluorescence results, we probed the mechanism of CDDP@Zr-MOF mediated inhibition of angiogenesis in the tumor microenvironment and further improve the sensitivity of A549R cells to cisplatin in RT. We used western blotting to quantify protein expression associated with angiogenesis and drug resistance in different groups. Significant hypoxia improvement and inhibition of angiogenic pathways were observed in the CDDP@Zr-MOF + RT treatment group, in which PI3K/AKT/mTOR/VEGF plays a leading role in angiogenesis and MRP1 protein expression was suppressed simultaneously (Fig. 4a). We compared related indicators quantitatively and found that key factors associated with angiogenesis were significantly suppressed in the CDDP@Zr-MOF + RT group. Notably, the VEGF inhibition rate was most obvious and the expression level of VEGF in the CDDP@Zr-MOF + RT group was inhibited nearly 6-fold compared with that in cisplatin and RT groups. Moreover, the amount of Akt protein expressed in angiogenesis related factors also had a significant inhibitory effect compared with the rest of the control group in the

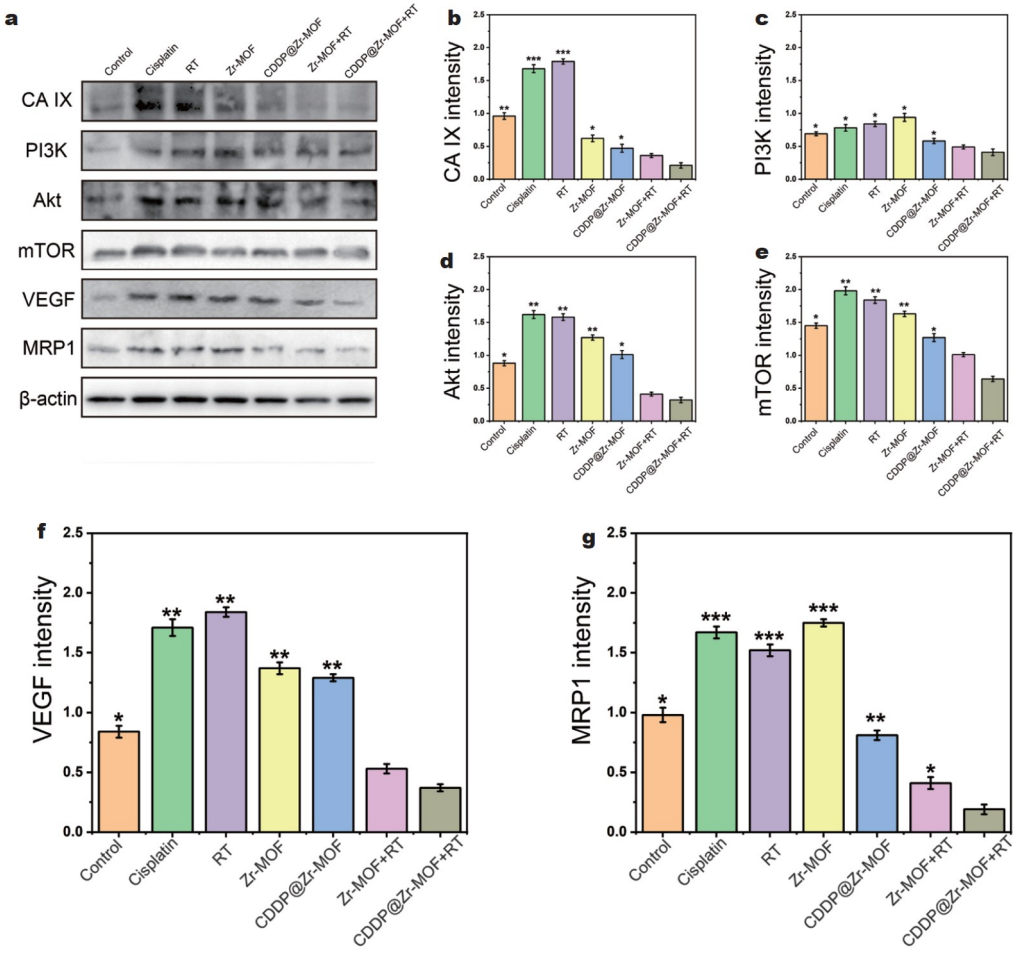

Figure 4 Mechanisms of angiogenesis inhibition mediated by CDDP@Zr-MOF + RT in cisplatin resistant A549 cells. (a) Western blotting results of angiogenesis related pathways induced by different treatments including PI3K/AKT/mTOR/VEGF combined with MRP1. (b–g) Relative expression levels associated with key proteins in (a) such as PI3K, AKT, mTOR, VEGF and MRP1 (* represents the statistical difference between the control group and the treatment groups). Data are presented as the mean ± SD. * $p < 0.05$; ** $p < 0.01$; *** $p < 0.001$.

CDDP@Zr-MOF + RT group and the inhibitory rate of PI3K and mTOR in the combined group had a greater inhibitory effect compared with the control group. Finally, the quantitative comparison of drug-resistant proteins showed that the content of MRP1 in the CDDP@Zr-MOF + RT group was significantly lower compared with other groups (Fig. 4b–f). The conclusions of related protein were consistent with polymerase chain reaction (PCR) in gene level of related factors (Fig. S12). The main reason for MRP1 inhibition was that hyperangiogenesis, of which VEGF is one of the most representative factor, was blocked in the tumor microenvironment. Zr-MOF can cascade in the tumor microenvironment through the following steps. First, the degradation products in an acidic surrounding can effectively inhibit the expression of hypoxia factor CAIX and then downregulate HIF-1α/CAIX/VEGF signaling; second, because VEGF was decreased, angiogenesis in tumor cells was inhibited. PI3K/AKT/mTOR/VEGF signaling was inhibited in a positive feedback modulated manner. Finally, MRP1 associated with the PI3K/AKT/mTOR/VEGF pathway was suppressed and cisplatin efflux was reduced from A549R cells, accompanied with the increased sensitivity of tumor cells to chemotherapeutic drugs and the improvement of therapeutic effect in RT. The CDDP@Zr-MOF + RT combination can effectively change the microenvironment of tumor cells in a cascade response by a collaborative mechanism, reverse drug resistance, and increase the sensitivity of combination therapy, thereby providing a comprehensive treatment strategy in cisplatin-resistant A549 cells. Moreover, we found that apatinib + CDDP@Zr-MOF + RT could more effectively inhibit the expression of VEGF and reverse the expression of MRP1. This maybe caused by the excellent vascular targeting effect of apatinib and the rapid microenvironmental response characteristics induced by MOF nanoparticles. Therefore, the strategy of loading apatinib into the CDDP@Zr-MOF structure maybe used to overcome cisplatin resistance through dual anti-angiogenesis mechanism in A549R cells in future (Figs S13 and S14).

Targeting effect of CDDP@Zr-MOF *in-vivo*

To evaluate the targeting ability of CDDP@Zr-MOF *in-vivo*, we used the CT imaging technique, which is an important diagnostic performance due to its deep tissue penetration and high resolution. CDDP@Zr-MOF has high Zr and Pt content, making it possible to use in based dynamic micro-CT (DMCT) monitoring on the basis of passive targeting. As shown in Fig. 5a, b,

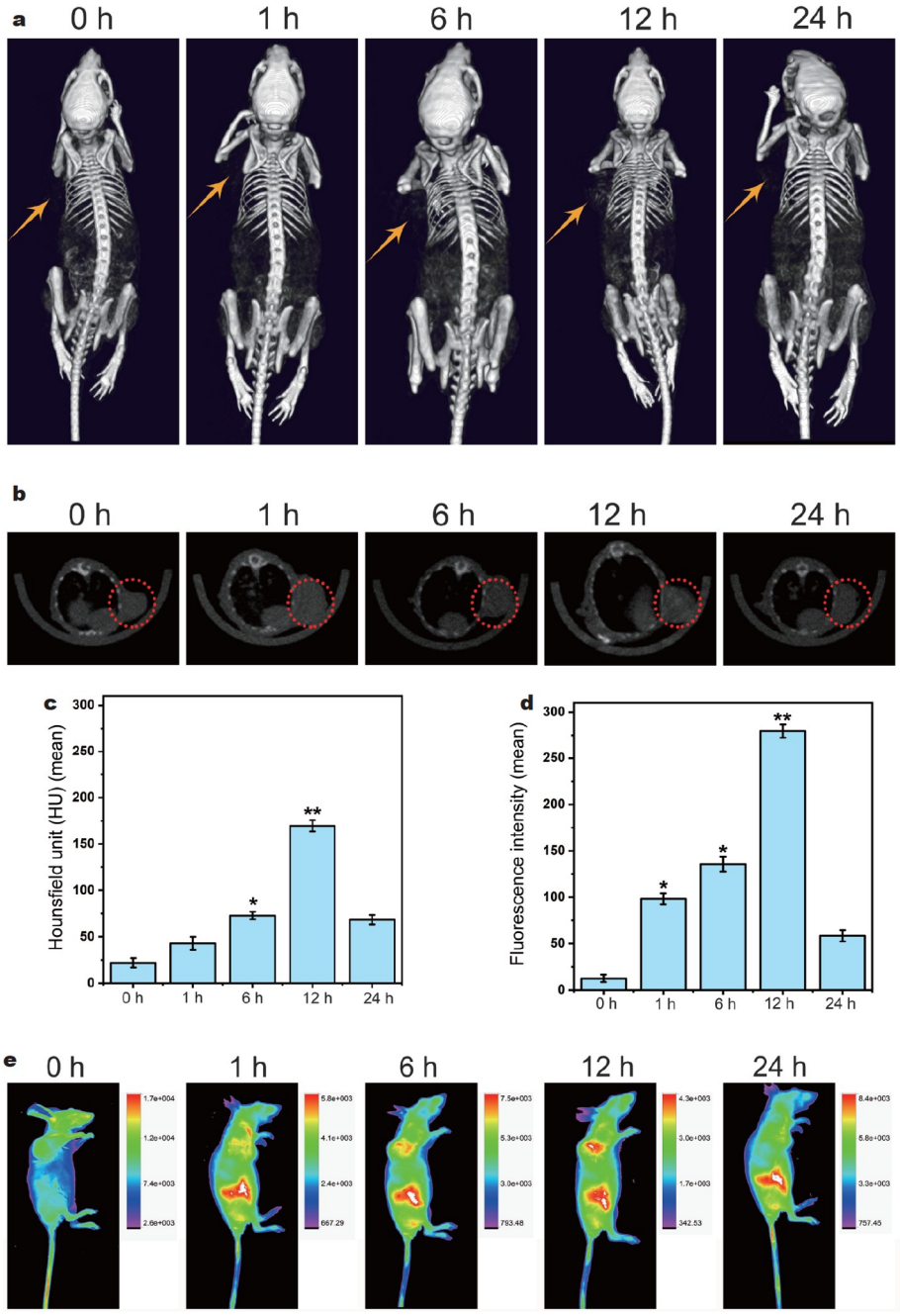

Figure 5 Directly tracking drug fate of CDDP@Zr-MOF *via* DMCT imaging and Xenogen *in vivo* imaging systems (IVIS) spectrum in cisplatin resistant A549 mice model. (a, b) *In vivo* CT images of mice for 0, 1, 6, 12, 24 h after intravenous administration (CDDP@Zr-MOF, 10 mg kg^{-1}). The CT signals are calculated in the range of red border. (c, d) Relative corresponding HU values and fluorescence intensity for 0, 1, 6, 12, 24 h after intravenous administration (CDDP@Zr-MOF, 10 mg kg^{-1}). (e) Fluorescence images of mice received CDDP@Zr-MOF-cy5.5 for different time intervals (n = 6). Data are presented as the mean ± SD. $^{*}p < 0.05$; $^{**}p < 0.01$.

1 h after injection of 10 mg kg^{-1} CDDP@Zr-MOF, high-density dots were seen in tumors of mice bearing A549R model. Several high-density dots emerged and persisted in the tumor areas with scanning time. The highest dot intensity was seen at 12 h, indicating the long circulation ability of CDDP@Zr-MOF, in both 3D images and axial images. High-density dots in the tumor indicated the penetration of CDDP@Zr-MOF to the tumor core. To quantify nanoparticles, we used hounsfield unit (HU) value by CT to assess the targeting effect. The relative pattern of CDDP@Zr-MOF distribution was specific. A gradual increase in HU signals for A549R tumor cells was observed with time from 0 h (21.98 HU) to 1 h (42.87 HU), 6 h (72.88 HU), 12 h (169.51 HU), and 24 h (68.4 HU) (Fig. 5c). *In vivo* imaging demonstrated the same results as that of DMCT scan, showing a more prominent fluorescence intensity in the tumor area. A gradual increase in fluorescence signals for A549R tumor could be observed with time; from 0 to 1, 6, 12, and 24 h at 12.58 to 98.26, 135.84, 279.60, and 58.41 μW cm^{-2}, respectively (Fig. 5d, e). All imaging results indicated that CDDP@Zr-MOF had excellent tumor targeting ability.

Anticancer efficacy of CDDP@Zr-MOF + RT in A549R models

Due to the superior tumor suppressive efficiency obtained *in-vitro* on A549R cells, we verified the efficacy *in-vivo* by using A549R BALB/c nude mice with tumor and the grouping was consistent with *in-vitro* experiments. The concentration of CDDP@Zr-MOF was 1 mg mL. We sacrificed all nude mice and compared them among seven groups after treatment. Subsequently, both tumor volumes and weights were calculated until 21 days (Fig. 6a, b). A549R tumors in control groups exhibited more than 5.9-fold increase of average tumor volume, compared with their original volumes, regardless of intervention options. Free cisplatin, RT, and Zr-MOF groups exhibited 3.7-, 3-, and 4.1-fold increase of tumor volume on A549R tumors, respectively, showing that free cisplatin and RT alone had a mediocre therapeutic effect on A549R cells due to cisplatin resistance and lower efficacy of Zr-MOF. However, CDDP@Zr-MOF + RT resulted in a remarkable influence on the growth of A549R tumors, demonstrating that CDDP@Zr-MOF itself has a non-negligible influence on tumor growth by altering hypoxia and angiogenesis in the local tumor microenvironment. RT plays an irreplaceable role in enhancing the function of cisplatin in A549R cells as well. Gross and tumor images of mice also exhibited changes among seven groups (Fig. 6c). Interestingly, CDDP@Zr-MOF and Zr-MOF + RT groups displayed 57.5% and 61.4% tumor compared with control group of inhibition rates on A549R tumors, respectively. Moreover, the CDDP@Zr-MOF + RT group could significantly delay tumor progression after 3 d, and there was no recurrence. The final anticancer rate

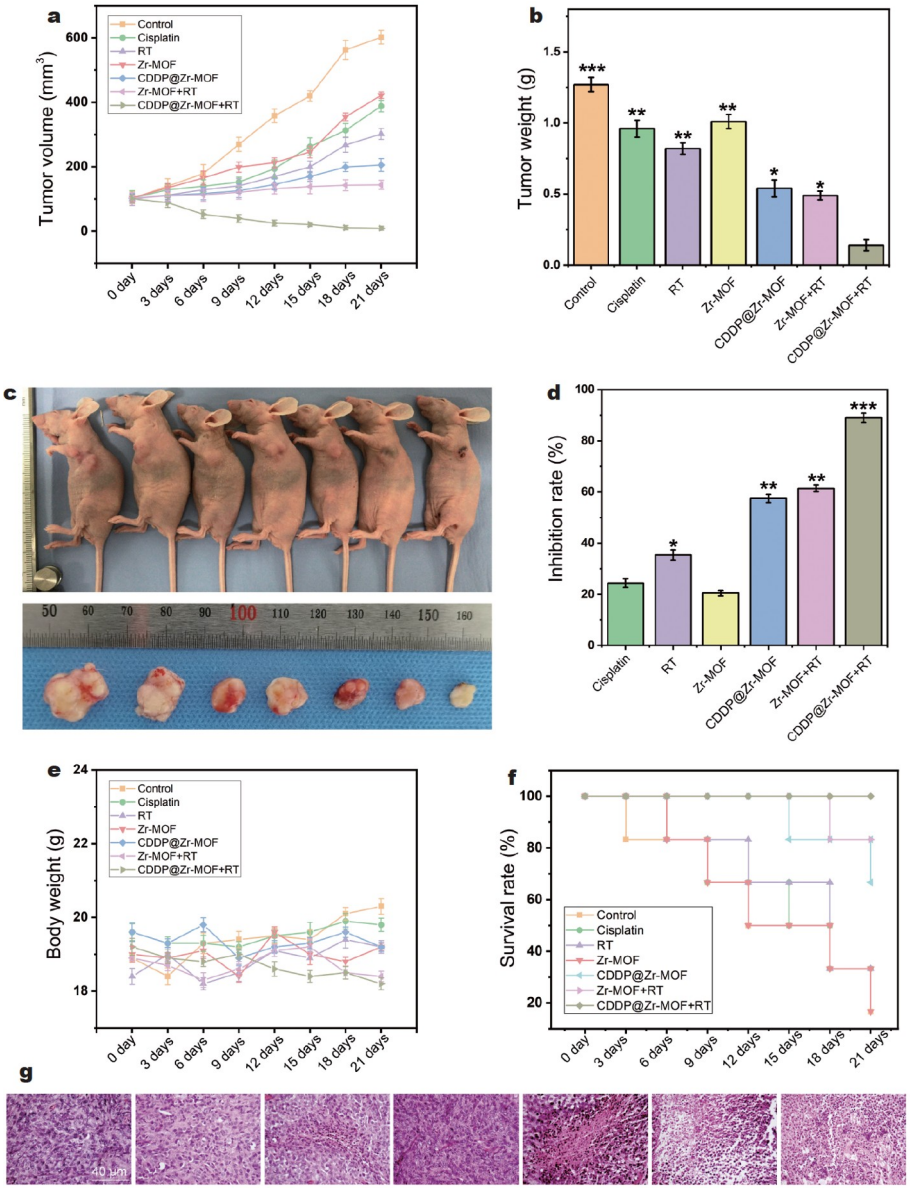

Figure 6 *In vivo* therapeutic outcomes induced by CDDP@Zr-MOF + RT in cisplatin resistant A549 tumor-bearing BALB/c nude mice. (a) Relative tumor growth curves of different treatment groups after 21 days in A549R mice. (b) Tumor weights of different groups showing in A549R mice. (c) Representative photographs in seven groups on 21 days. (d) Tumor inhibition rates in combination group and other groups. (e) Body weight of A549R mice at the end of each treatment. (f) Survival profiles at the end of each treatment in A549R. (g) Images of H&E-stained A549R tumor sections harvested from the mice treated with CDDP@Zr-MOF + RT and other control groups (scale bar: 40 μm. The representative images were 400X. * represents the statistical difference between the treatment groups and the control group). $n = 6$ in each group, data are expressed as mean ± SD. * $p < 0.05$; ** $p < 0.01$; *** $p < 0.001$.

of the combination treatment was 89%. The combination group demonstrated the difference compared with the cisplatin and Zr-MOF groups ($p < 0.001$), compared with the RT group ($p < 0.01$) and compared with CDDP@Zr-MOF, Zr-MOF + RT groups ($p < 0.05$) (Fig. 6d). During treatment, no mice died in the combination group, indicating that the CDDP@Zr-MOF + RT strategy could achieve better survival benefits with significantly prolonged survival time (Fig. 6f). There were no obvious body weight changes in all groups (Fig. 6e). We collected A549R tumor sections for hematoxylin and eosin (H&E) staining for all treatments. CDDP@Zr-MOF + RT treatment resulted in more severe cancer necrosis with extensive damage accompanied by increased necrosis, cell morphologic changes, and apparently condensed nuclei, whereas single cisplatin and RT only caused slightly hemorrhagic inflammation and sporadic areas of necrosis. The Zr-MOF group exhibited a local inflammatory response and a small amount of tumor cell necrosis. Moderate amounts of tumor cell necrosis were detected in the remaining two groups (Fig. 6g). The excellent experimental results obtained by CDDP@Zr-MOF mediated RT were determined by the following factors: (1) Zr-MOF can effectively react in the acidic tumor microenvironment. The decomposition product can inhibit the expression of key factor CAIX, leading to the blocking of the HIF-1α/CAIX/VEGF pathway, thereby inhibiting intracellular angiogenesis. (2) VEGF expression was reduced, which resulted in PI3K/AKT/mTOR/VEGF signaling being blocked in the tumor microenvironment in positive feedback manner by CDDP@Zr-MOF + RT co-operating function, leading to the downregulation of the most important drug-resistant protein MRP1. (3) Increase in intracellular cisplatin content changed the sensitivity of A549 cells to cisplatin combining with RT and further synergistically enhance treatment effect. Thus, CDDP@Zr-MOF + RT might act as an effective strategy to ablate A549R model *in-vivo* without regrowth through a microenvironment-responsive nano-system. Moreover, we found that combination with apatinib could induce tumor necrosis more effectively, leading to more pronounced tumor shrinkage (Figs S15 and S16).

Comparison of immunohistochemical analysis *in-vivo*

Immunohistochemical analysis was operated in cisplatin-resistant A549R mice after treatment in seven groups. We focused on factors related to hypoxia, angiogenesis, and apoptosis in the tumor microenvironment, including HIF-1α, CAIX, CD31, VEGF, PI3K, AKT, mTOR, and TUNEL. We found that HIF-1α and CAIX exhibited lower relative expression in the combination group, which was consistent with the previous conclusions, indicating that Zr-MOF was capable of significantly inhibiting signaling of hypoxic pathways (Figs 7 and 8a, b). As a marker to evaluate the activity of neovascularization in the tumor, we detected the expression levels of CD31 and VEGF in cisplatin A549R mice of each group. We found that the levels of CD31

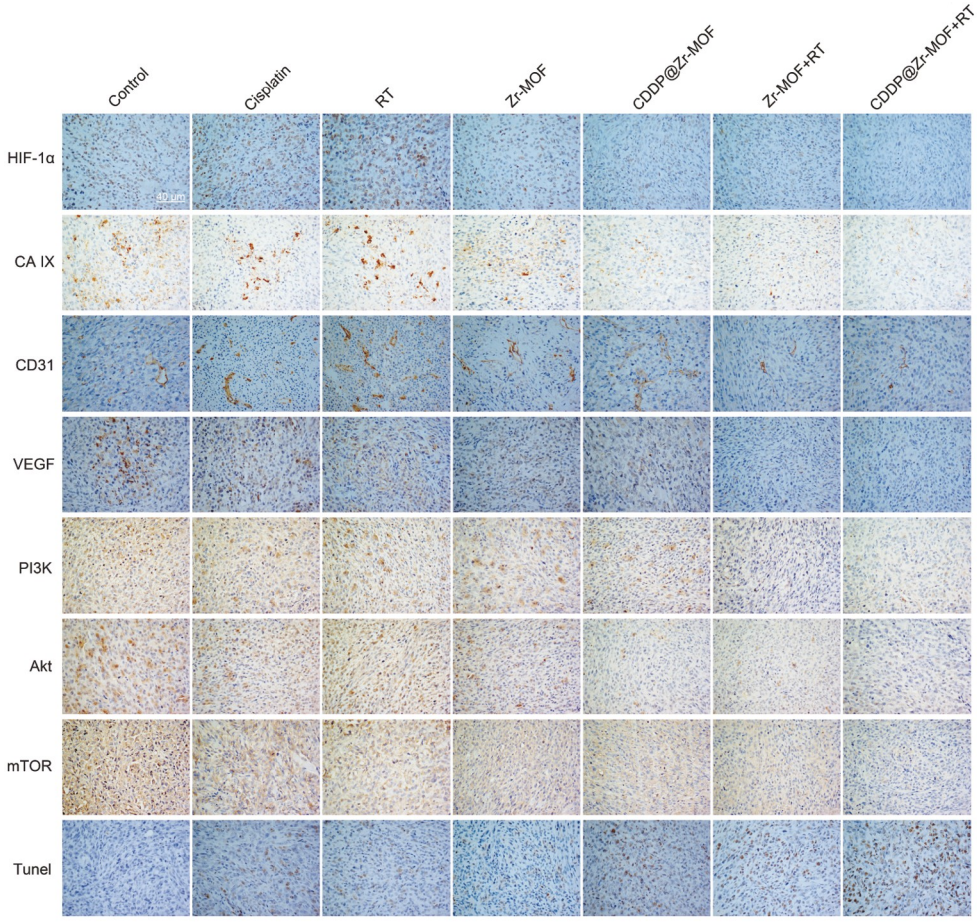

Figure 7 Immunohistochemical analysis of tumor tissues in cisplatin resistant A549 mice after treatment in different groups. The expression levels of HIF-1α, CAIX, CD31, VEGF, PI3K, AKT, mTOR, and TUNEL in seven groups, respectively.

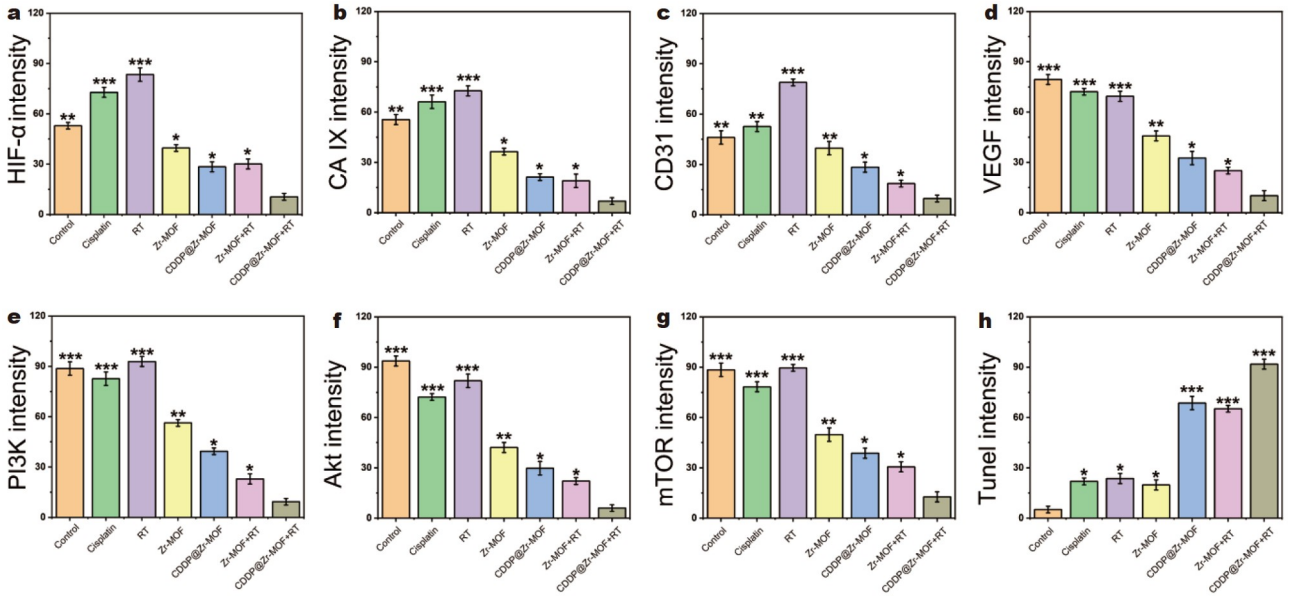

Figure 8 Expression levels of HIF-1α (a), CAIX (b), CD31 (c), VEGF (d), PI3K (e), AKT (f), mTOR (g), and TUNEL (h) in seven groups, respectively (* represents the statistical difference between the treatment groups and the control group). * $p < 0.05$; ** $p < 0.01$; *** $p < 0.001$.

and VEGF in the CDDP@Zr-MOF + RT group exhibited the lowest expression compared with control, cisplatin, and RT groups, indicating that the combined treatment group had a strong ability to inhibit angiogenesis, and other groups had different degrees of inhibition of angiogenesis (Figs 7 and 8c, d). Moreover, because neovascularization was inhibited, the PI3K/AKT/mTOR pathway also controlled signaling. We found that differences in expression levels were similar to the results of VEGF in seven groups (Figs 7 and 8e–g). However, the expression of TUNEL in combination group was the maximum, far more than that in CDDP@Zr-MOF and Zr-MOF + RT groups. The comparison of cisplatin and RT groups did not show significant differences (Figs 7 and 8h). Zr-MOF as a VEGF inhibitor can improve neovascularization in tumor tissues by silencing CAIX, which is indispensable for gene regulation. The hypoxic pathway and angiogenic pathway intersect; therefore, the alteration of hypoxic factors in the microenvironment may cause a series of biological behavior changes in tumor cells. In this research, we used CDDP@Zr-MOF + RT to figure cisplatin-resistant A549 mice by performing changing hypoxia, inhibiting angiogenesis, reversing drug resistance, enhancing RT sensitization, and promoting apoptosis. Finally, CDDP@Zr-MOF + RT combined with apatinib could induce expression change of related factors and the trend was similar to previous results (Figs S17 and S18).

Mechanisms of angiogenesis inhibition mediated by CDDP@Zr-MOF + RT *in-vivo*

Based on immunohistochemical semi-quantitative analysis in A549R mice, we found that the CDDP@Zr-MOF + RT group can significantly inhibit angiogenesis and reduce apoptosis in tumors. We used real-time PCR and western blotting to quantify protein levels associated with hypoxia, angiogenesis, and drug resistance in different groups. The results revealed that significant hypoxia improvement and inhibition of angiogenic pathways were observed in the combination treatment group, in which CAIX, VEGF, and MRP1 expressions were suppressed simultaneously (Fig. 9a). We further compared the three indicators quantitatively, and found that VEGF, associated with angiogenesis, and CAIX, associated with hypoxia, were significantly suppressed in the CDDP@Zr-MOF + RT group; the expression of VEGF and CAIX in combination group was inhibited nearly 4- and 5-fold compared with control and cisplatin groups, respectively. Finally, the quantitative comparison of drug-resistant proteins revealed that the content of MRP1 in the CDDP@Zr-MOF + RT group was significantly reduced compared with other groups (Fig. 9b–d). This change was consistent at the gene level, as seen by PCR analysis (Fig. S19). CDDP@Zr-MOF + RT can effectively regulate the microenvironment of A549R *in-vivo* in a cascade response and reverse drug resistance as a VEGF inhibitor, thereby increasing the sensitivity of chemoradiotherapy. Furthermore, apatinib + CDDP@Zr-MOF + RT could more effectively inhibit VEGF expression and further reverse the expression of MRP1. This may correlate to excellent vascular inhibition mediated by apatinib and responsive characteristics reacted from Zr-MOF nanoparticles and hypoxia microenvironment, inducing controlled VEGF expression. Therefore, we established a strategy to overcome cisplatin resistance mediated by the dual anti-angiogenesis mechanism in A549R tumor-bearing BALB/c nude mice (Fig. S20).

Safety evaluation of CDDP@Zr-MOF *in-vivo*

We evaluated the toxicity of CDDP@Zr-MOF in mice. All pathological assays of major organs and hematological and biochemical tests were performed. No significant abnormal behavior was observed in A549R bearing mice throughout the experiment, confirming the excellent biocompatibility of CDDP@Zr-MOF (Fig. S21). Similarly, changes in all functional indicators can be controlled, which was suggested by the slight steady standard of biomarkers listed in Figs S22 and S23. Therefore, we believe that our results support the feasibility of

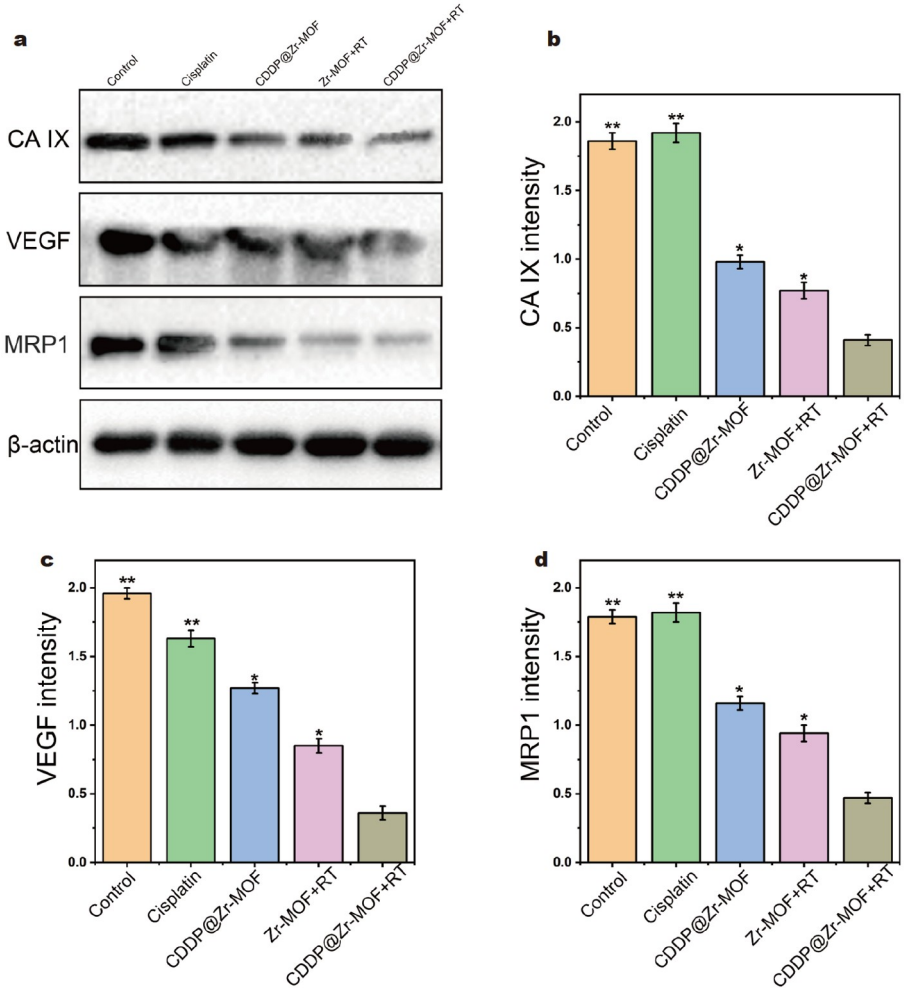

Figure 9 Mechanisms of angiogenesis inhibition mediated by CDDP@Zr-MOF + RT in cisplatin resistant A549 mice. (a) Western blotting results of angiogenesis related protein VEGF combined with hypoxia-associated protein CAIX and MRP1. (b–d) Relative expression levels associated with key proteins such as VEGF, CAIX, and MRP1. All the experiments were repeated three times. Data are presented as the mean ± SD (* represents the statistical difference between the treatment groups and the control group). * $p < 0.05$; ** $p < 0.01$; *** $p < 0.001$.

employing CDDP@Zr-MOF in the clinic with RT. Apatinib also has some side effects, and the main side effects are hypertension, proteinuria, hand-foot syndrome, diarrhea, in addition to fatigue, mouth ulcers and hoarseness.

CONCLUSIONS

In conclusion, to reverse chemotherapy resistance in tumor cells, we designed CDDP@Zr-MOF and combined it with RT for treating cisplatin-resistant A549 cells. This multifunctional drug-delivery system displayed a chain-shattering manner under intracellular or acidic microenvironment for optimal anticancer efficacy, targeting hypoxia properties efficiently, inhibiting tumor angiogenesis, blocking PI3K/AKT/mTOR pathway, reversing MRP1 expression, and improving the sensitivity of A549R cells to cisplatin and RT. Moreover, Zr-MOF@CDDP can be applied as a contrast agent to directly track the drug *via* DMCT and fluorescence scanning *in-vivo*. The cascade strategy was used to treat A549R cells by using CDDP@Zr-MOF + RT without significant side effects. Our results provided an example of microenvironment response nanomedicine in tackling drug resistance in tumors, including precise release, microenvironmental remodeling, real-time monitoring, and therapeutic effect evaluation. Our study leads to further research into the use of CDDP@Zr-MOF + RT in biomedical applications.

Received 15 November 2023; accepted 13 January 2024; published online 12 April 2024

1 Vasan N, Baselga J, Hyman DM. A view on drug resistance in cancer. Nature, 2019, 575: 299–309
2 Chen Q, Chen J, Yang Z, *et al.* Nanoparticle-enhanced radiotherapy to trigger robust cancer immunotherapy. Adv Mater, 2019, 31: 1802228
3 Chen Q, Xu L, Liang C, *et al.* Photothermal therapy with immune-adjuvant nanoparticles together with checkpoint blockade for effective cancer immunotherapy. Nat Commun, 2016, 7: 13193
4 Xu J, Xu L, Wang C, *et al.* Near-infrared-triggered photodynamic therapy with multitasking upconversion nanoparticles in combination with checkpoint blockade for immunotherapy of colorectal cancer. ACS Nano, 2017, 11: 4463–4474
5 Zhang LN, Xin T, Chen M, *et al.* Chemoresistance in mesenchymal lung cancer cells is correlated to high regulatory T cell presence in the tumor microenvironment. IUBMB Life, 2019, 71: 986–991
6 Naghizadeh S, Mohammadi A, Baradaran B, *et al.* Overcoming multiple drug resistance in lung cancer using siRNA targeted therapy. Gene,

2019, 714: 143972
7 Yang G, Xu L, Chao Y, *et al.* Hollow MnO_2 as a tumor-microenvironment-responsive biodegradable nano-platform for combination therapy favoring antitumor immune responses. Nat Commun, 2017, 8: 902
8 Xu J, Lv J, Zhuang Q, *et al.* A general strategy towards personalized nanovaccines based on fluoropolymers for post-surgical cancer immunotherapy. Nat Nanotechnol, 2020, 15: 1043–1052
9 Xing Y, Liu Y, Liu T, *et al.* TNFAIP8 promotes the proliferation and cisplatin chemoresistance of non-small cell lung cancer through MDM2/p53 pathway. Cell Commun Signal, 2018, 16: 43
10 Li Y, Deng Y, Tian X, *et al.* Multipronged design of light-triggered nanoparticles to overcome cisplatin resistance for efficient ablation of resistant tumor. ACS Nano, 2015, 9: 9626–9637
11 Fang L, Qin X, Zhao J, *et al.* Construction of dual stimuli-responsive platinum(IV) hybrids with NQO1 targeting ability and overcoming cisplatin resistance. Inorg Chem, 2019, 58: 2191–2200
12 Bao X, Sun Y, Bao C, *et al.* Design, synthesis and evaluation of *N*-hydroxypropenamides based on adamantane to overcome resistance in NSCLC. Bioorg Chem, 2019, 86: 696–704
13 Liu W, Du Y, Wen R, *et al.* Drug resistance to targeted therapeutic strategies in non-small cell lung cancer. Pharmacol Ther, 2020, 206: 107438
14 Zhao H, Xu J, Li Y, *et al.* Nanoscale coordination polymer based nanovaccine for tumor immunotherapy. ACS Nano, 2019, 13: 13127–13135
15 Tang Z, Liu Y, He M, *et al.* Chemodynamic therapy: Tumour microenvironment-mediated Fenton and Fenton-like reactions. Angew Chem Int Ed, 2019, 58: 946–956
16 Zhuang W, Xu Y, Li G, *et al.* Redox and pH dual-responsive polymeric micelles with aggregation-induced emission feature for cellular imaging and chemotherapy. ACS Appl Mater Interfaces, 2018, 10: 18489–18498
17 Zheng DW, Lei Q, Zhu JY, *et al.* Switching apoptosis to ferroptosis: Metal–organic network for high-efficiency anticancer therapy. Nano Lett, 2017, 17: 284–291
18 Dong X, Pan P, Zheng DW, *et al.* Bioinorganic hybrid bacteriophage for modulation of intestinal microbiota to remodel tumor-immune microenvironment against colorectal cancer. Sci Adv, 2020, 6: 1590
19 Xu Y, Han X, Li Y, *et al.* Sulforaphane mediates glutathione depletion *via* polymeric nanoparticles to restore cisplatin chemosensitivity. ACS Nano, 2020, 13: 13445–13455
20 Zheng DW, Dong X, Pan P, *et al.* Phage-guided modulation of the gut microbiota of mouse models of colorectal cancer augments their responses to chemotherapy. Nat Biomed Eng, 2019, 3: 717–728
21 Zhang J, Chen C, Fu H, *et al.* MicroRNA-125a-loaded polymeric nanoparticles alleviate systemic lupus erythematosus by restoring effector/regulatory T cells balance. ACS Nano, 2020, 14: 4414–4429
22 Gadhave D, Gorain B, Tagalpallewar A, *et al.* Intranasal teriflunomide microemulsion: An improved chemotherapeutic approach in glioblastoma. J Drug Deliver Sci Tech, 2019, 51: 276–289
23 Akbarzadeh A, Rezaei-Sadabady R, Davaran S, *et al.* Liposome: Classification, preparation, and applications. Nanoscale Res Lett, 2013, 8: 102
24 Zhang Y, Dong Y, Fu H, *et al.* Multifunctional tumor-targeted PLGA nanoparticles delivering Pt(IV)/siBIRC5 for US/MRI imaging and overcoming ovarian cancer resistance. Biomaterials, 2021, 269: 120478
25 Xia Y, Sun J, Zhao L, *et al.* Magnetic field and nano-scaffolds with stem cells to enhance bone regeneration. Biomaterials, 2018, 183: 151–170
26 Li T, Wang P, Guo W, *et al.* Natural berberine-based Chinese herb medicine assembled nanostructures with modified antibacterial application. ACS Nano, 2019, 13: 6770–6781
27 Gong N, Zhang Y, Teng X, *et al.* Proton-driven transformable nanovaccine for cancer immunotherapy. Nat Nanotechnol, 2020, 15: 1053–1064
28 Zeng X, Wang Y, Han J, *et al.* Fighting against drug-resistant tumors using a dual-responsive Pt(IV)/Ru(II) bimetallic polymer. Adv Mater, 2020, 32: 2004766
29 Yang B, Chen Y, Shi J. Exosome biochemistry and advanced nanotechnology for next-generation theranostic platforms. Adv Mater, 2019, 31: 1802896
30 Yue W, Chen L, Yu L, *et al.* Checkpoint blockade and nanosonosensitizer-augmented noninvasive sonodynamic therapy combination reduces tumour growth and metastases in mice. Nat Commun, 2019, 10: 2025
31 Xia D, Xu P, Luo X, *et al.* Overcoming hypoxia by multistage nanoparticle delivery system to inhibit mitochondrial respiration for photodynamic therapy. Adv Funct Mater, 2019, 29: 1807294
32 Dai L, Li X, Duan X, *et al.* A pH/ROS cascade-responsive charge-reversal nanosystem with self-amplified drug release for synergistic oxidation-chemotherapy. Adv Sci, 2019, 6: 1801807
33 Zhu W, Shan X, Wang T, *et al.* miR-181b modulates multidrug resistance by targeting BCL2 in human cancer cell lines. Intl J Cancer, 2010, 127: 2520–2529
34 Huo M, Wang L, Chen Y, *et al.* Tumor-selective catalytic nanomedicine by nanocatalyst delivery. Nat Commun, 2017, 8: 357
35 Cheng YJ, Hu JJ, Qin SY, *et al.* Recent advances in functional mesoporous silica-based nanoplatforms for combinational photo-chemotherapy of cancer. Biomaterials, 2020, 232: 119738
36 Jiang P, Xu H, Xu C, *et al.* NEAT1 contributes to the CSC-like traits of A549/CDDP cells *via* activating Wnt signaling pathway. Chem-Biol Interact, 2018, 296: 154–161
37 Zhang W, Zhang Z, Tung CH. Beyond chemotherapeutics: Cisplatin as a temporary buckle to fabricate drug-loaded nanogels. Chem Commun, 2017, 53: 779–782
38 Zhou R, Yan L, Dong X, *et al.* Fractionated regimen-suitable immunoradiotherapy sensitizer based on ultrasmall $Fe_4Se_2W_{18}$ nanoclusters enable tumor-specific radiosensitization augment and antitumor immunity boost. Nano Today, 2021, 36: 101003
39 Wang L, Gao F, Wang A, *et al.* Defect-rich adhesive molybdenum disulfide/rGO vertical heterostructures with enhanced nanozyme activity for smart bacterial killing application. Adv Mater, 2020, 32: 2005423
40 Yan L, Zhao F, Wang J, *et al.* Clinical nanomaterials: A safe-by-design strategy towards safer nanomaterials in nanomedicines. Adv Mater, 2019, 31: 1970325
41 Mautschke HH, Drache F, Senkovska I, *et al.* Catalytic properties of pristine and defect-engineered Zr-MOF-808 metal organic frameworks. Catal Sci Technol, 2018, 8: 3610–3616
42 Cong Y, Xiao H, Xiong H, *et al.* Dual drug backboned shattering polymeric theranostic nanomedicine for synergistic eradication of patient-derived lung cancer. Adv Mater, 2018, 30: 1706220
43 Wu X, Wu Y, Ye H, *et al.* Interleukin-15 and cisplatin co-encapsulated thermosensitive polypeptide hydrogels for combined immuno-chemotherapy. J Control Release, 2017, 255: 81–93
44 Chu PC, Wu YC, Chen CY, *et al.* Novel HIF-1α inhibitor CDMP-TQZ for cancer therapy. Future Med Chem, 2021, 13: 1057–1072
45 Wu H, Jin H, Wang C, *et al.* Synergistic cisplatin/doxorubicin combination chemotherapy for multidrug-resistant cancer *via* polymeric nanogels targeting delivery. ACS Appl Mater Interfaces, 2017, 9: 9426–9436
46 Min H, Wang J, Qi Y, *et al.* Biomimetic metal–organic framework nanoparticles for cooperative combination of antiangiogenesis and photodynamic therapy for enhanced efficacy. Adv Mater, 2019, 31: 1808200
47 Li Z, Di C, Li S, *et al.* Smart nanotherapeutic targeting of tumor vasculature. Acc Chem Res, 2019, 52: 2703–2712
48 Wang B, Ding Y, Zhao X, *et al.* Delivery of small interfering RNA against Nogo-B receptor *via* tumor-acidity responsive nanoparticles for tumor vessel normalization and metastasis suppression. Biomaterials, 2018, 175: 110–122
49 Ma T, Liu Y, Wu Q, *et al.* Quercetin-modified metal–organic frameworks for dual sensitization of radiotherapy in tumor tissues by inhibiting the carbonic anhydrase IX. ACS Nano, 2019, 13: 4209–4219

Acknowledgements This work was supported by the National Natural Science Foundation of China (82172041 and 81801808), Harbin Medical University Cancer Hospital Haiyan Foundation (JJZD202101, JJQN2019-02,

and JJZD2018-02), Heilongjiang Postdoctoral Fund (LBH-Z18160 and LBH-TZ2018), the Natural Science Foundation of Heilongjiang (YQ2023H023 and LH2020H127), and Heilongjiang Province Youth Innovative Talents Training Program (UNPYSCT-2020162).

Author contributions Song C, Xie C, and Guan X designed and performed the experiments, analyzed the data, and wrote the manuscript. Wu Q provided the technical or material support. Jiang S and Hong Z conducted the data analysis and gave insightful suggestions and comments on the outline of this manuscript. Qu G, Ma T, and Cui Y supervised the entire project, obtained the fundings, designed the experiments, and revised the manuscript. All authors read and approved the final manuscript.

Conflict of interest The authors declare that they have no conflict of interest.

Supplementary information Supporting data are available in the online version of the paper.

Chunyu Song received his master's degree in oncology from Harbin Medical University (2014). His primary focus is on clinical diagnosis, treatment, and fundamental research of bone and soft tissue tumors.

Guofan Qu received his PhD degree in oncology from Harbin Medical University in 2007. Prof. Qu is currently a chief physician and doctoral supervisor at the Department of Orthopedics, Harbin Medical University Cancer Hospital, focusing on clinical diagnosis, treatment, and basic research of bone tumors and soft tissue tumors.

利用金属有机框架抑制PI3K/AKT/mTOR信号传导通路以克服放化疗中的多重耐药性

宋春雨[1†], 关雪[2†], 谢昌明[3†], 姜珊[4], 洪智文[4], 吴琼[5], 曲国蓄[1*], 马腾闯[4*], 崔亚利[4*]

摘要 肿瘤微环境中的血管生成是肿瘤细胞对放化疗不敏感的主要原因. 在本项研究中, 我们设计了一种微环境响应型的纳米颗粒, 利用Zr-MOF的分解产物抑制肿瘤细胞中的PI3K/AKT/mTOR/VEGF通路, 从而克服A549R细胞对顺铂的耐药性. 我们将顺铂包裹在Zr-MOF中, 并在表面修饰BSA, 形成了CDDP@Zr-MOF-BSA纳米复合体, 该复合体在肿瘤微环境中有良好的响应性, 有助于在肿瘤区域蓄积, 展现出卓越的血管生成抑制能力, 并能明显降低药物的外排. 此外, CDDP@Zr-MOF-BSA能显著抑制多药耐药相关蛋白1 (MRP1)的表达, 从而逆转A549R细胞的耐药性. 总体而言, CDDP@Zr-MOF-BSA对A549R有细胞毒性, 能抑制肿瘤微环境中的血管生成, 最终有效提高顺铂耐药肿瘤的治疗效果. CDDP@Zr-MOF-BSA为放化疗治疗耐药肿瘤提供了一种多功能协同的方法.